# Doppler-enhanced FMCW LiDAR odometry based on linear continuous-time representation

Weitong Wu 1, Chi Chen 2,3,4 \*, Bisheng Yang 2,3,4, Yuhang Xu 2,3,4, Yueqian Shen 1, Xiufeng He 1

<sup>1</sup> School of Earth Sciences and Engineering, Hohai University, Nanjing 211100, China – (weitongwu, y.shen\_lidar, xfhe)@hhu.edu.cn

<sup>4</sup> Institute of Geo-spatial intelligence, Wuhan University, Wuhan 430079, China

#### Abstract:

LiDAR-based simultaneous localization and mapping (SLAM) plays a crucial role in applications such as search and rescue, infrastructure inspection, and underground exploration. However, conventional LiDAR-based methods often exhibit significantly reduced accuracy in degenerate environments. To address this challenge, this paper proposes a simple yet effective linear continuous-time FMCW (Frequency-Modulated Continuous Wave) LiDAR odometry method that tightly integrates Doppler constraints and point-to-plane constraints within a sliding-window-based factor graph optimization framework. The proposed method is comprehensively validated using datasets collected from a vehicle equipped with an Aeva I FMCW LiDAR in both typically degenerate scenes and highway scenarios. Experimental results demonstrate that the proposed method achieves the lowest trajectory root mean square error (RMSE) among the three sequences out of the total eight sequences, outperforming all compared methods. Notably, on Sequence 7, which spans an approximately trajectory length of 7,300 m, our method achieves a minimum trajectory RMSE of 10.19 m.

Keywords: Unmanned systems, FMCW LiDAR, LiDAR odometry, Doppler measurements, Linear continuous-time

#### 1. Introduction

As a fundamental technology for unmanned systems, LiDAR SLAM (Simultaneous Localization and Mapping) enables precise pose estimation and environmental reconstruction through sequential point cloud registration, finding essential applications in search and rescue, infrastructure inspection and underground space exploration (Zhao et al., 2024; Yang et al., 2025). The seminal breakthrough in 3D LiDAR odometry was achieved by LOAM (Zhang and Singh, 2014). As of the time of writing, LOAM maintains its position as the top-ranked LiDARonly method on the KITTI Odometry Benchmark. Subsequent research has produced various methodological extensions (Zhang et al., 2024). To address the challenges posed by high-dynamic motions, CT-ICP (Dellenbach et al., 2022) introduced a linear continuous-time LiDAR odometry framework considering intrascan pose continuity and inter-scan discontinuity. Building on this, Traj-LO (Zheng and Zhu, 2024) developed a slidingwindow optimization that tightly couples the geometric constraints from LiDAR points with trajectory smoothness constraints. Wu et al. (2023a) proposed an adaptive frame length LiDAR odometry that dynamically adjusts the frame length through analysis of the motion state and matching features.

Conventional LiDAR odometry frameworks exhibit significantly reduced accuracy or even failure in feature-sparse scenarios such as tunnels, long corridors, and open terrains, due to insufficient stable geometric features for robust scan matching (Chen et al., 2024). Although degeneracy-aware strategies have been developed for point cloud registration, such approaches can only mitigate rather than completely eliminate the effects of geometric degeneracy (Tuna et al., 2024; Wu et al., 2025). To address this limitation, the emerging frequency-modulated continuous wave (FMCW) LiDAR technology (Zhang et al., 2020) presents a promising advancement by integrating Doppler velocity measurements alongside traditional geometric data, thereby providing complementary motion constraints that could enhance state estimation reliability under challenging environments. Hexsel et al. (2022) pioneered Doppler ICP (DICP) algorithm using FMCW LiDAR, incorporating radial velocity and geometric constraints into a joint optimization framework to

enable robust point cloud registration in feature-denied environments. While their work focused on discrete registration frameworks, Wu et al. (2023b) introduced the first continuous-time FMCW LiDAR odometry, named STEAM-DICP, which uses Gaussian process regression for refined trajectory estimation. Addressing the computational bottleneck in STEAM-DICP, Pang et al. (2024) proposed an efficient Doppler LiDAR odometry based on IESKF (Iterative Error State Kalman Filter) framework, through temporal scan slicing and vehicle kinematic modelling. Currently, the number of relevant studies is limited.

In this paper, we propose a simple yet effective linear continuoustime FMCW LiDAR odometry method that tightly integrates Doppler constraints and point-to-plane geometric constraints, differing from Wu et al.'s (2023b) approach. To mitigate approximation errors induced by linear motion assumptions, the frame duration is sliced below the conventional 100ms. A sliding window optimization framework is implemented, incorporating three key constraints: marginalized prior constraints from historical states, geometric constraints of downsampled LiDAR points to the map, and Doppler velocity constraints of downsampled LiDAR points.

The remainder of the paper is structured as follows. Section 2 introduces the proposed doppler-enhanced FCMW LiDAR odometry. Section 3 details the validation datasets and experimental results while also delineating the methodological limitations and prospective research avenues. The conclusion is outlined in Section 4.

### 2. Methodology

Our method takes FMCW LiDAR frames as input and estimates the continuous-time trajectory by employing sliding-window-based factor graph optimization. Figure 1 illustrates the workflow of our proposed method. Firstly, a single frame point cloud data (typically acquired within 100 ms) is segmented and reorganized into smaller, temporally equal segments based on a predefined segment duration, in contrast to the work by Lin and Zhang (2020). Therefore, any remaining data will be segmented with the subsequent frame. Subsequently, a factor graph incorporating

<sup>&</sup>lt;sup>2</sup> State Key Laboratory of Information Engineering in Surveying, Mapping and Remote Sensing, Wuhan University, Wuhan 430079, China- (chichen, bshyang, yuhangxu)@whu.edu.cn

<sup>&</sup>lt;sup>3</sup> Engineering Research Center for Spatio-temporal Data Smart Acquisition and Application, Ministry of Education of China, Wuhan University, Wuhan 430079, China

<sup>\*</sup> Corresponding author: Chi Chen (chichen@whu.edu.cn)

"Mobile Mapping for Autonomous Systems and Spatial Intelligence", 20-22 June 2025, Xiamen, China

geometric constraints, Doppler constraints and marginalization constraints is constructed and optimized based on Gauss-Newton

method. Finally, the voxel map employed for point cloud matching is updated.

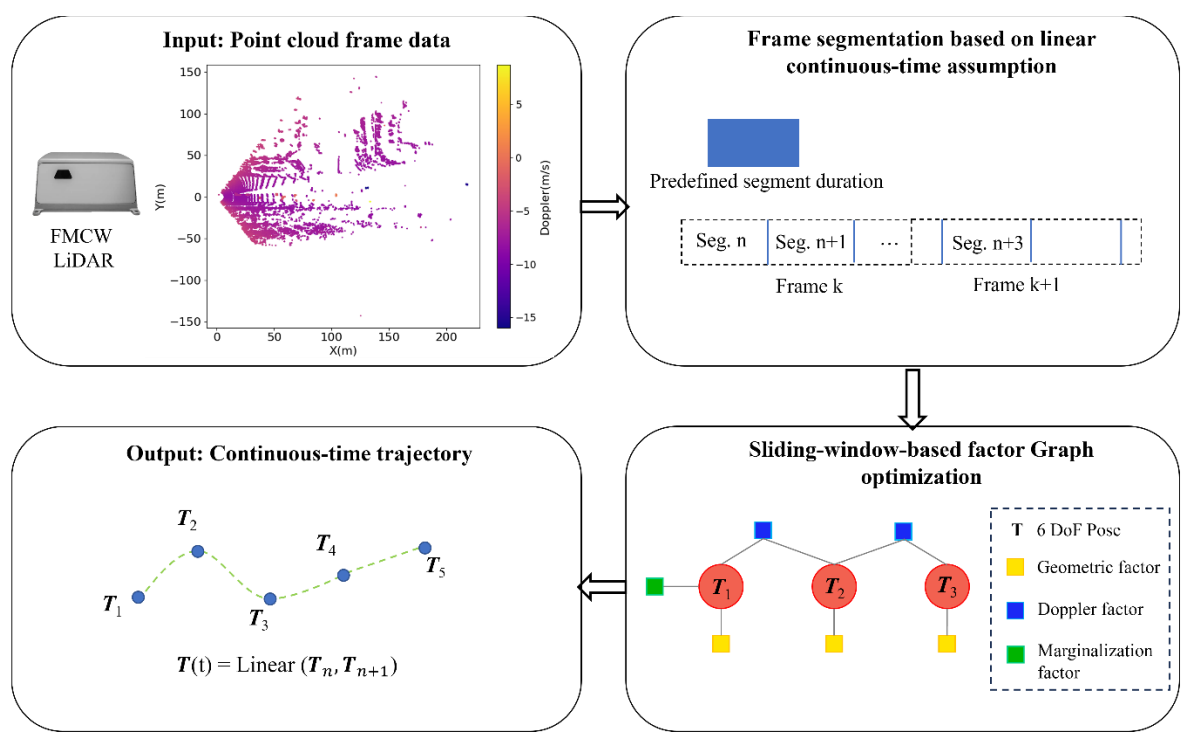


Figure 1. Workflow of the proposed FMCW LiDAR odometry. The system takes the FMCW LiDAR point cloud as input and outputs the continuous-time local trajectory. Firstly, a single frame point cloud data is segmented into smaller segments to better approximate the linear motion assumption. Subsequently, a sliding-window-based factor graph incorporating LiDAR point-to-plane factors, Doppler factors and a marginalization factor is constructed and optimized. Finally, the voxel map is updated using the estimated pose, which is not depicted in the figure.

# 2.1 Frame Segmentation Based on Linear Continuous-time Assumption

Continuous-time trajectory representation, in contrast to discrete-time representation, enables simultaneous point cloud distortion correction and motion estimation, offering a more rigorous approach. A linear motion assumption is employed within each segment. The duration of these segments  $\Delta t$  is determined based on the movement status, typically less than the frame duration, generally providing a better approximation of the linear motion assumption.

Suppose the poses at the start and end time of any segment are  $T_s$  and  $T_e$ , respectively; then, any pose T(t) within this segment duration can be computed as:

$$T(t) = T_s \exp\left(\frac{t - t_s}{t_e - t_s} \log(T_s^{-1} T_e)\right), \tag{1}$$

where  $t_s$  and  $t_e$  are the start and end times of the segment, respectively, and  $\exp(\cdot)$  and  $\log(\cdot)$  denote the exponential and logarithm maps of the SE(3).

#### 2.2 Sliding-Window-Based Factor Graph Optimization

To balance efficiency and accuracy, a sliding-window-based factor graph is maintained. The window contains K segments. The state vector  $\mathbf{X} = \{T_1, T_2, ..., T_{K+1}\}$  consists of the poses associated to these segments. The start and end pose of each segment are optimized. For example, if K = 2, then the number of poses to be optimized is 3. When a new segment is added to the factor graph, the oldest segment is removed. Subsequently, a

marginalization prior factor is derived to retain information from the segment removed from the window.

The geometric factor is derived by matching downsampled LiDAR points to the closest locally fitted plane in the voxel map. Unlike discrete-time methods, there is no need for motion distortion correction beforehand. The LiDAR point-to-plane residual  $e_{geometric}$  can be computed as:

$$e_{geometric} = \mathbf{u}_i^n \cdot \mathbf{T}(t_i^n) \mathbf{p}_i^n + d_i^n, \tag{2}$$

where  $\boldsymbol{p}_i^n$  denotes the *i*-th raw point in the *n*-th segment.  $\boldsymbol{T}(t_i^n)$  denotes the pose of the point at its acquisition time  $t_i^n$  using equation (1), and  $\{\boldsymbol{u}_i^n,d_i^n\}$  represents the coefficient of the closest plane in the voxel map of  $\boldsymbol{p}_i^n$ . Here,  $\boldsymbol{u}_i^n$  is the normal vector of the plane, and  $d_i^n$  is the distance from the origin to the plane.

The Doppler factor is derived from the geometric relationship between the Doppler measurement d and the system velocity:

$$d = -\mathbf{v} \cdot \frac{\mathbf{p}}{\|\mathbf{p}\|},\tag{3}$$

where v denotes the system velocity in the coordinate frame at the time  $t_p$ . Therefore, the Doppler factor can be computed as:

$$e_{doppler} = d + \mathbf{R}_{s}^{-1} \frac{\mathbf{p}_{e} - \mathbf{p}_{s}}{\Delta t} \cdot \frac{\mathbf{p}}{\|\mathbf{p}\|}, \tag{4}$$

where  $p_s$  and  $R_s$  are the translation and rotation part of  $T_s$ , respectively. To accelerate the optimization process, only the Doppler measurements from the downsampled LiDAR points are utilized to construct Doppler factors. Owing to the linear motion

assumption, the system velocity at the  $t_p$  can be directly derived from the velocity at the start time of the segment.

The cost function E of the corresponding factor graph can be represented as:

$$E(X) = E_{geometric} + E_{doppler} + E_{margin}, \tag{5}$$

where  $E_{geometric}$  and  $E_{doppler}$  denote the sum of the least-squares form of the residuals  $e_{geometric}$  and  $e_{doppler}$ , respectively.  $E_{margin}$  can be referred to in Zheng and Zhu (2024). The cost function is optimized using the Gauss-Newton method.

# 3. Experiment Results

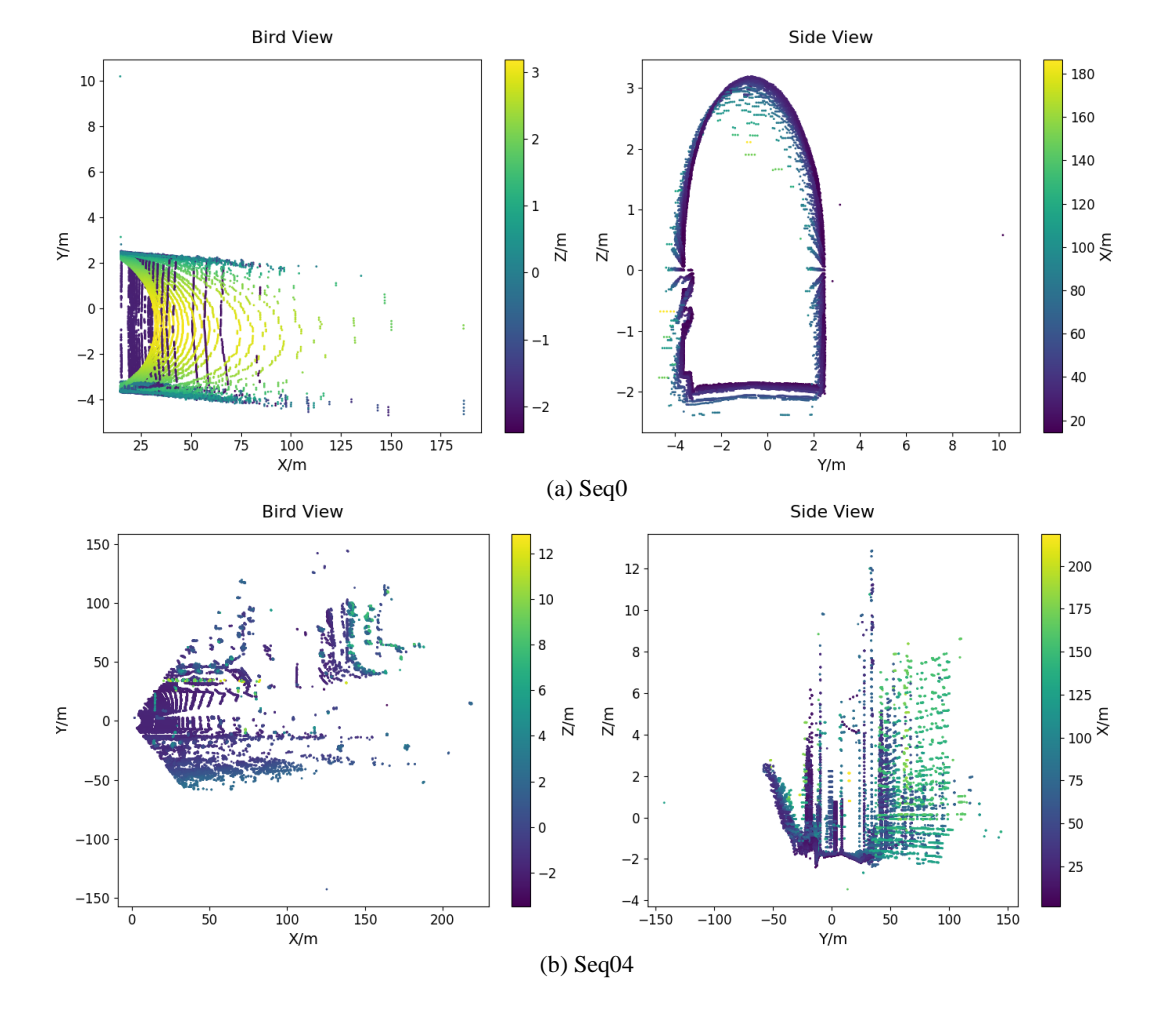
We evaluated our method's performance on real-world FMCW LiDAR sequences from Wu et al. (2023b), acquired using an Aeva Aeries I sensor featuring: 120°(H) × 30°(V) FoV, 300 m maximum range, 3 cm/s Doppler precision, and 10 Hz sampling rate. The Aeva dataset, comprising eight sequences that cover

urban tunnels and highway scenarios, was used for a comparative analysis against state-of-the-art approaches, including CT-ICP (Dellenbach et al., 2022), Trja-LO (Zheng and Zhu, 2024) and STEAM-DICP (Wu et al., 2023b). Sequences 0-3 exhibit fewer geometric features with correspondingly shorter trajectories, whereas Sequences 4-7 contain moderate geometric characteristics with longer trajectories. Table 1 shows the dataset description. Figure 2 presents sample 3D LiDAR data of representative scenes from the dataset.

Traj-LO and our method were implemented by C++ and tested on a computer equipped with an Intel i7-14700K CPU and 64G RAM. The segment duration  $\Delta t$  was set to 40 ms, and the segment number K was set to 3. The results for CT-ICP and STEAM-DICP were calculated using the trajectory provided by Wu et al. (2023b).

	Trajectory length/m	Num. of frames	Characteristics		
Seq0	860	837	Tunnal magn accompanie		
Seq1	907	658	Tunnel, poor geometric features		
Seq2	689	301	reatures		
Seq3	4942	1762			
Seq4	8876	6343	Freeway/Highway/		
Seq5	7836	4734	Parkway, moderate		
Seq6	10310	5083	geometric features		
Seq7	7328	4012	-		

Table 1. Dataset description.



"Mobile Mapping for Autonomous Systems and Spatial Intelligence", 20-22 June 2025, Xiamen, China

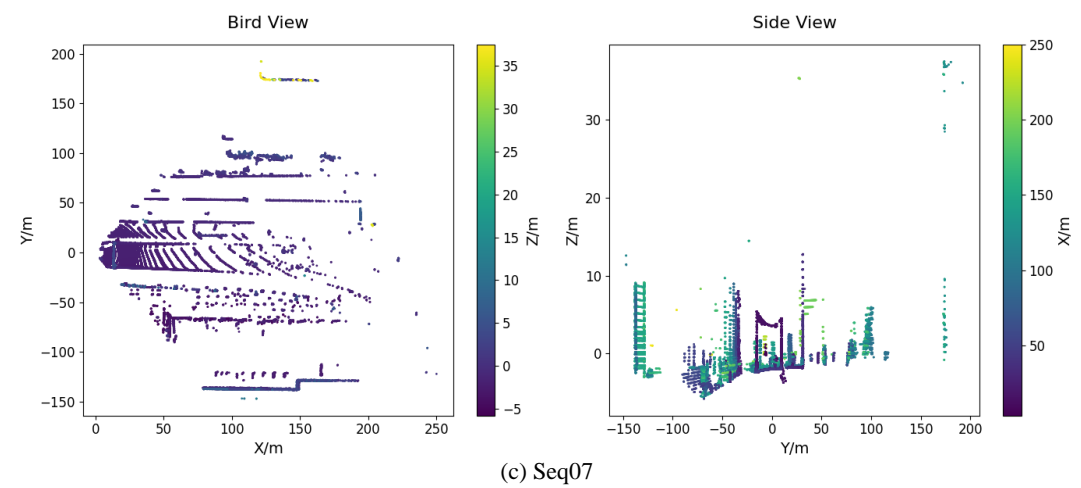


Figure 2. Comparative LiDAR scene representations in the Aeva dataset.

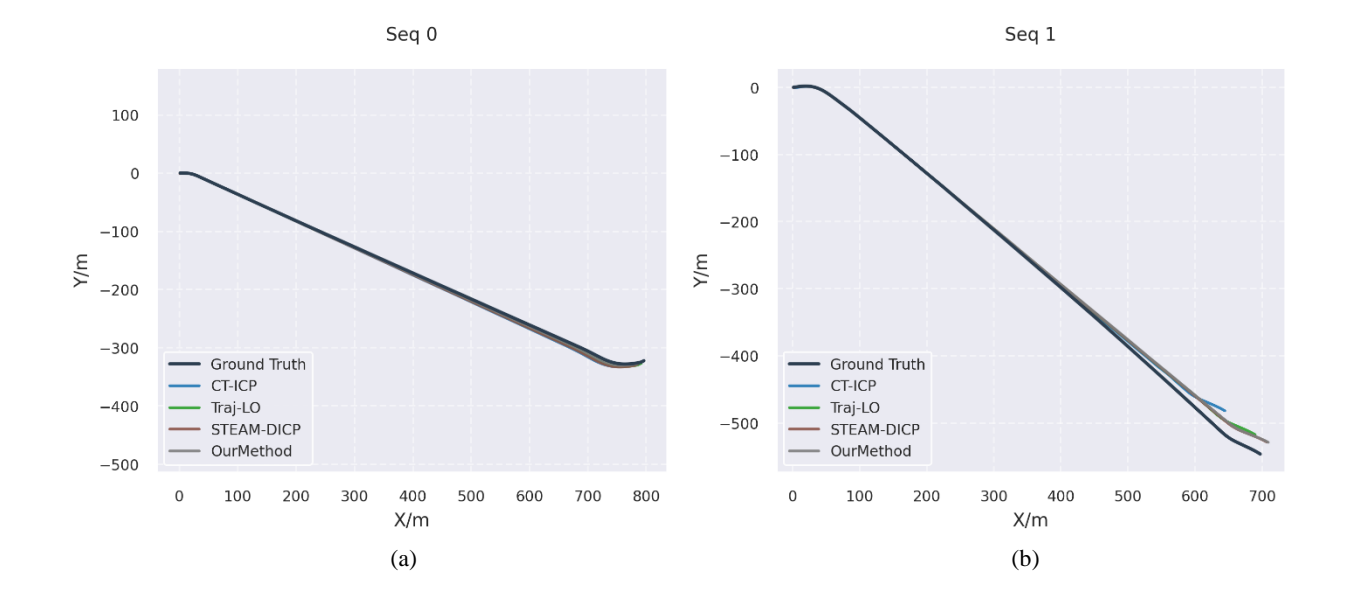
Aeva dataset	Seq0	Seq1	Seq2	Seq3	Seq4	Seq5	Seq6	Seq7
CT-ICP	4.79	28.55	15.94	11.65	33.61	14.69	38.2	33.32
Traj-LO	2.22	13.81	36.09	17.23	28.0	10.72	54.29	<u>14.76</u>
STEAM-DICP	3.31	3.14	0.93	24.62	<u>17.16</u>	47.41	23.13	43.03
Our Method	2.53	2.95	1.11	22.27	16.27	21.45	36.85	10.19

Table 2. Trajectory RMSE comparison on test sequences (unit: meters). Bold indicates best results; underline indicates second-best results.

Table 2 compares the root mean square errors (RMSE) of absolute trajectory error (ATE) on the test sequences. We calculated the ATE with the evo tool, performing Umeyama alignment based on all trajectory points between the evaluated trajectories with the ground truth. Our method achieves the lowest RMSE results among the three sequences, which is the best among all the compared methods. On Sequence 1 and 2, CT-ICP and Traj-LO demonstrate significantly higher localization errors compared to Doppler-enhanced methods, quantitatively validating the effectiveness of Doppler velocity constraints in degraded scenarios. On Sequence 7 with approximately 7,300 m trajectory length, our method achieves the minimum trajectory RMSE of 10.19 m. On Sequence 6, Traj-LO achieves the largest trajectory RMSE of 54.29 m, as high-dynamic motions in this sequence violate the trajectory smoothness assumption.

Figure 3 demonstrates the trajectories estimated by our method and baseline methods on the Aeva dataset. For better visualization and comparison, we performed Umeyama alignment based on the first 200 trajectory points. Quantitative metrics in Table 2 demonstrate strong alignment with the trajectory result in Figure 3, whereas discrepancies are observed specifically in Sequence 4. This phenomenon can be attributed to the Umeyama alignment before ATE calculation. It is suggested to integrates ATE metric with qualitative trajectory visualization to holistically assess algorithm performance.

There still exists room for improvement in our method. In future work, we plan to adaptively adjust the frame length to handle more complex motion dynamics with the assisting of Doppler measurements.



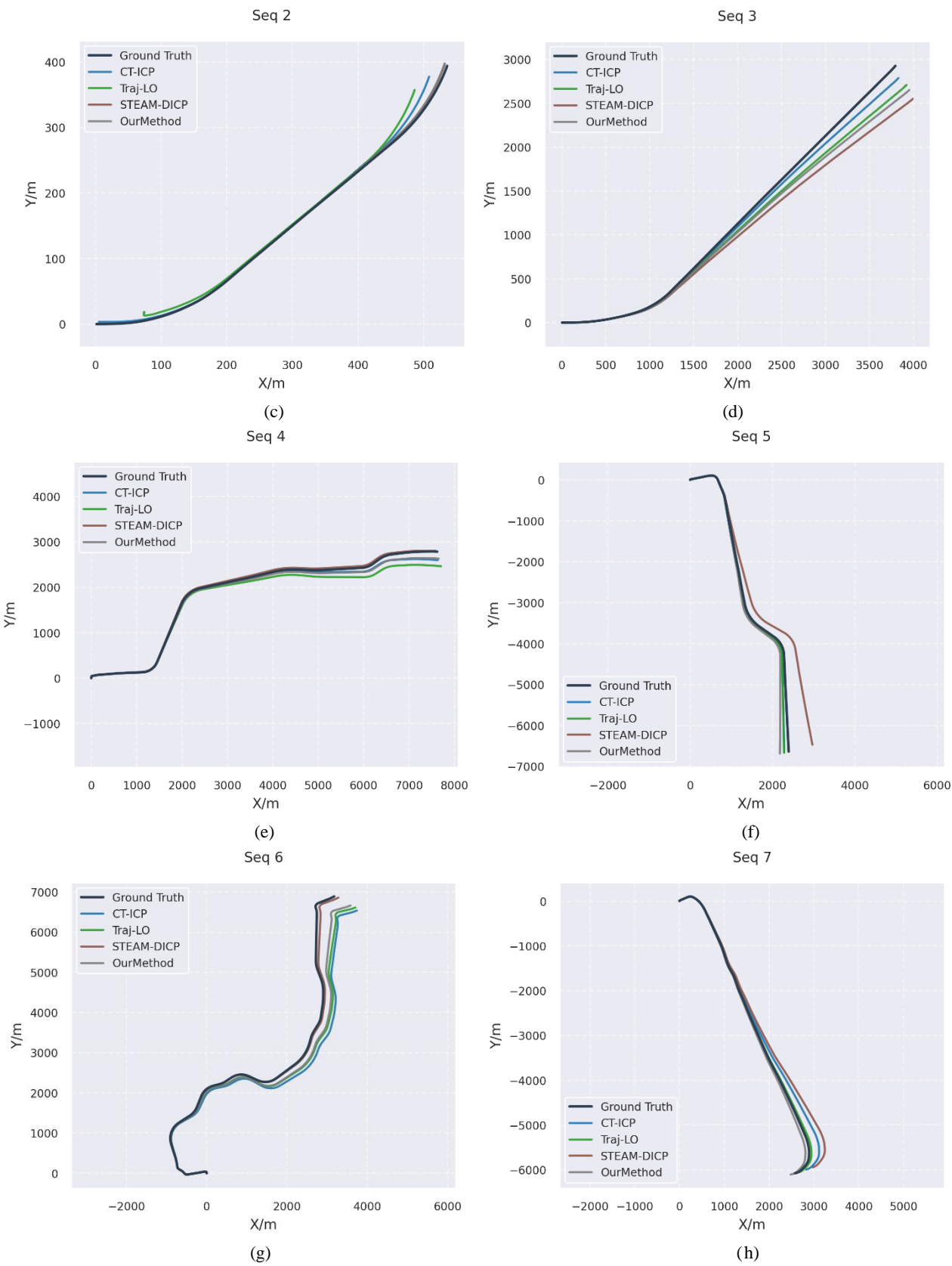


Figure 3. Trajectories estimated by our method and baseline methods on the Aeva dataset. Subfigures (a)-(h) correspond to Seq0 through Seq7, respectively.

"Mobile Mapping for Autonomous Systems and Spatial Intelligence", 20-22 June 2025, Xiamen, China

#### 4. Conclusion

FMCW LiDAR is a promising perception technology capable of acquiring dense point clouds along with additional Doppler measurements. However, due to its higher cost, there have been relatively few studies on LiDAR odometry utilizing this technology. This paper proposes a simple yet effective FMCW LiDAR odometry approach to better handle degenerate scenes such as tunnels. The core idea is to segment each frame into smaller segments to better approximate the linear motion assumption. In the future, it is anticipated that Doppler measurements will be utilized more effectively.

#### Acknowledgements

This research was jointly funded by the National Natural Science Foundation of China (Nos. 42401538; U22A20568) and the Fundamental Research Funds for the Central Universities (No. B240201098).

#### References

Chen, Z., Qi, Y., Feng, D., Zhuang, X., Chen, H., Hu, X., ... & Lu, P., 2024. Heterogeneous lidar dataset for benchmarking robust localization in diverse degenerate scenarios. arXiv preprint arXiv:2409.04961.

Dellenbach, P., Deschaud, J. E., Jacquet, B., & Goulette, F. (2022, May). Ct-icp: Real-time elastic lidar odometry with loop closure. In 2022 International Conference on Robotics and Automation (ICRA) (pp. 5580-5586). IEEE.

Hexsel, B., Vhavle, H., Chen, Y., 2022. Dicp: Doppler iterative closest point algorithm. arXiv preprint arXiv:2201.11944.

Lin J, Zhang F, 2020. Loam livox: A fast, robust, high-precision LiDAR odometry and mapping package for LiDARs of small FoV[C]//2020 IEEE international conference on robotics and automation (ICRA). IEEE, pp. 3126-3131.

Pang, C., Shen, Z., Wu, R., Fang, Z., 2024. Efficient Doppler LiDAR Odometry using Scan Slicing and Vehicle Kinematics. IEEE Transactions on Instrumentation and Measurement, 1–1. DOI: 10.1109/TIM.2024.3509599.

Tuna, T., Nubert, J., Pfreundschuh, P., Cadena, C., Khattak, S., & Hutter, M., 2024. Informed, constrained, aligned: A field analysis on degeneracy-aware point cloud registration in the wild. arXiv preprint arXiv:2408.11809.

Wu, W., Chen, C., Yang, B., Zou, X., Liang, F., Xu, Y., & He, X., 2025. DALI-SLAM: Degeneracy-aware LiDAR-inertial SLAM with novel distortion correction and accurate multiconstraint pose graph optimization. ISPRS Journal of Photogrammetry and Remote Sensing, 221, 92-108.

Wu, W., Li, J., Chen, C., Yang, B., Zou, X., Yang, Y., ... & Chen, R., 2023a. AFLI-Calib: Robust LiDAR-IMU extrinsic self-calibration based on adaptive frame length LiDAR odometry. ISPRS Journal of Photogrammetry and Remote Sensing, 199, 157-181.

Wu, Y., Yoon, D.J., Burnett, K., Kammel, S., Chen, Y., Vhavle, H., Barfoot, T.D., 2023b. Picking up Speed: Continuous-Time Lidar-Only Odometry Using Doppler Velocity Measurements. IEEE Robotics and Automation Letters, 8, 264–271. https://doi.org/10.1109/LRA.2022.3226068.

Yang B S, Sun S Z, Chen C., 2025. Autonomous non-exposed space exploration based on unmanned system. National Remote Sensing Bulletin, online. https://doi.org/10.11834/jrs.20254330.

Zhang, J., & Singh, S. (2014, July). LOAM: Lidar odometry and mapping in real-time. In Robotics: Science and systems (Vol. 2, No. 9, pp. 1-9).

Zhang, F., Yi, L., Qu, X., 2020. Simultaneous measurements of velocity and distance via a dual-path FMCW lidar system. Optics communications, 474, 126066.

Zhang, Y., Shi, P., & Li, J. (2024). 3d lidar slam: A survey. The Photogrammetric Record, 39(186), 457-517.

Zhao X., Liang F., Li J., Chen Y., Yang B., 2024. 3D Detection of Extraterrestrial Lava Tunnels Based on Lightweight Mobile Measurement System and Surface Verification on Earth. Journal of Deep Space Exploration, 11(4): 385-393. DOI: 10.15982/j.issn.2096-9287.2024.20230143.

Zheng, X., Zhu, J., 2024. Traj-lo: In defense of lidar-only odometry using an effective continuous-time trajectory. IEEE Robotics and Automation Letters, 2, 1961–1968.